coatings

MDPI

Article

Hardness and Wettability Characteristics of Electrolytically Produced Copper Composite Coatings Reinforced with Layered Double Oxide (Fe/Al LDO) Nanoparticles

Samah Sasi Maoloud Mohamed [1], Nebojša D. Nikolić [2], Marija M. Vuksanović [3,*], Rastko Vasilić [4], Dana G. Vasiljević-Radović [2], Radmila M. Jančić Heinneman [1], Aleksandar D. Marinković [1] and Ivana O. Mladenović [2,*]

[1] Faculty of Technology and Metallurgy, University of Belgrade, Karnegijeva 4, 11 000 Belgrade, Serbia; samahsasi1@gmail.com (S.S.M.M.); radica@tmf.bg.ac.rs (R.M.J.H.); marinko@tmf.bg.ac.rs (A.D.M.)
[2] Institute of Chemistry, Technology and Metallurgy, University of Belgrade, Njegoševa 12, 11 000 Belgrade, Serbia; nnikolic@ihtm.bg.ac.rs (N.D.N.); dana@nanosys.ihtm.bg.ac.rs (D.G.V.-R.)
[3] Department of Chemical Dynamics, and Permanent Education, "VINČA" Institute of Nuclear Sciences—National Institute of the Republic of Serbia, University of Belgrade, Mike Petrovića Alasa, 11 000 Belgrade, Serbia
[4] Faculty of Physics, University of Belgrade, Studentski Trg 12-16, 11 000 Belgrade, Serbia; rastko.vasilic@ff.bg.ac.rs
* Correspondence: marija.vuksanovic@vin.bg.ac.rs (M.M.V.); ivana.mladenovic@ihtm.bg.ac.rs (I.O.M.); Tel.: +381-11-262-85-87 (I.O.M.)

Abstract: The lab-made ferrite-aluminium layered double oxide (Fe/Al LDO) nanoparticles were used as reinforcement in the production of copper matrix composite coatings via the electrodeposition route in this study. The Cu coatings electrodeposited galvanostatically without and with low concentrations of Fe/Al LDO nanoparticles were characterized by SEM (morphology), AFM (topography and roughness), XRD (phase composition and texture), Vickers microindentation (hardness), and the static sessile drop method (wettability). All Cu coatings were fine-grained and microcrystalline with a (220) preferred orientation, with a tendency to increase the grain size, the roughness, and this degree of the preferred orientation with increasing the coating thickness. The cross-section analysis of coatings electrodeposited with Fe/Al LDO nanoparticles showed their uniform distribution throughout the coating. Hardness analysis of Cu coatings performed by application of the Chicot-Lesage (C-L) composite hardness model showed that Fe/Al LDO nanoparticles added to the electrolyte caused a change of the composite system from "soft film on hard cathode" into "hard film on soft cathode" type, confirming the successful incorporation of the nanoparticles in the coatings. The increase in roughness had a crucial effect on the wettability of the coatings, causing a change from hydrophilic reinforcement-free coatings to hydrophobic coatings obtained with incorporated Fe/Al LDO nanoparticles.

Keywords: copper coatings; co-electrodeposition; Fe/Al layered double oxide; morphology; structure; microindentation; composite hardness model; wettability

Citation: Sasi Maoloud Mohamed, S.; Nikolić, N.D.; Vuksanović, M.M.; Vasilić, R.; Vasiljević-Radović, D.G.; Jančić Heinneman, R.M.; Marinković, A.D.; Mladenović, I.O. Hardness and Wettability Characteristics of Electrolytically Produced Copper Composite Coatings Reinforced with Layered Double Oxide (Fe/Al LDO) Nanoparticles. *Coatings* **2024**, *14*, 740. https://doi.org/10.3390/coatings14060740

Academic Editors: Walter Ricardo Brito and Yonny Romaguera Barcelay

Received: 8 May 2024
Revised: 2 June 2024
Accepted: 9 June 2024
Published: 11 June 2024

1. Introduction

Electrochemical deposition of metals has been used as a technique to modify their surface, making them resistant to the working environment. In recent years, the longevity of such materials, prolonging their use, and reducing the need for new raw materials have been at the center of modern responsible research [1]. Copper is frequently chosen due to its good corrosion resistance, and the possibility of serving as a matrix for various kinds of reinforcement that can improve the properties of the material and the coating. Research on thin copper films has primarily focused on their microstructural and electrical characteristics, leveraging copper's favorable attributes such as high melting temperature, resistance to electromigration, and low electrical resistivity [2]. Electrochemical deposition

methods, including electrodeposition and co-electrodeposition techniques, have been extensively studied to enhance the structural, mechanical, and electrical properties of copper coatings and their composites [3].

In industrial applications, direct current (DC) electrodeposition is preferred over pulse current (PC) due to advantages such as lower complexity, reduced equipment costs, shorter plating times, and higher efficiency [4]. Copper coatings and their intermetallic composites are utilized in various applications, including electrocatalysts, anode current collectors, and chip interconnections [5,6].

The selection of particle types in the metal matrix is crucial for functionalization and application possibilities. For instance, wear-resistant composite coatings with metallic Ni matrices containing SiC particles [7] or Cu/diamond composite coatings exhibit excellent thermal transport properties and wear/hardness resistance [8]. Moreover, ultra-thin copper matrix composites with MXene as a second phase have proven effective for electromagnetic interference shielding [9]. Copper-thin films also demonstrate antibacterial and antiviral properties [10]. Additionally, through the electrodeposition of copper in a deep eutectic solvent, superhydrophobic coatings with self-cleaning capability and ultrahigh corrosion resistance have been formed [11]. Various strategies have been employed to enhance the hardness, anti-wear, and corrosion-resistant properties of metallic films and alloys. One approach involves incorporating or doping microparticles into metallic matrices as reinforcing phases [12]. To enhance the hardness of the copper matrix, hard ceramic particles such as SiC [13], TiN [14], Si_3N_4 [15], Cr_2O_3 [16], ZrO_2 [17], Al_2O_3 [18], WC [19], and diamond particles [3] are added. The microstructure, encompassing carbides, nitrides, and oxides, can also be refined.

Layered double hydroxides (LDHs) are a class of bimetallic hydroxide compounds known for their ease of synthesis and versatile properties and uses. The LDH structure involves different metal combinations tailored to specific applications. Despite their widespread use, LDHs face drawbacks such as poor acid stability, instability in aqueous solutions, and susceptibility to agglomeration [20]. To overcome these limitations, various modification methods, such as calcination [21] and surface modification [22], are employed to enhance material performance. Layered double oxide (LDO) emerges through the calcination of LDH, featuring a more stable structure ideal for aquatic environment decontamination [22]. Throughout the heat treatment process, layered double hydroxides undergo a gradual loss of interlayer water molecules. Additionally, as the temperature rises, LDH experiences significant dehydroxylation and decarbonation, resulting in its transformation into layered double oxides [23]. In essence, LDH compounds decompose into a blend of oxides known as layered double oxides (LDOs). LDOs boast a higher theoretical capacity compared to LDHs, attributed to the absence of interlayer anions and water. The temperature during the preparation process plays a pivotal role in controlling particle size, size distribution, and shape [24].

Methods such as surface modification, calcination, compounding, and intercalation can achieve this transformation, rendering LDO particles resistant to acidic electrolytes. This can be achieved by calcining the synthesized LDH particles at a precisely determined temperature. Previous research has shown that LDO particles show a higher adsorption power compared to classical LDH particles, as shown in the examples of Mg/Al [25] and Zn/Al LDO particles [26] in the removal of Cr(VI). The application of these particles in the function of reinforced polymers and dental matrices was presented in the previous work [27,28]. Recent research suggests that Zn/Al LDH in pH-neutral titanium oxide oxalate $K_2TiO(C_2O_4)_2$ electrolyte in the PEO (plasma electrolyte oxidation) process is very interesting for photocatalytic application of these coatings [29] with improved anti-corrosion properties. A functionalization of this class of lamellar nanomaterials is presented [30], where the use of LDH particles as nanofillers in polylactic acid (PLA) for biomedical matrix is discussed. It is generally known that inorganic clays have a hydrophilic character, while PLA shows a hydrophobic character, resulting in poor mixing of the materials during the

synthesis of composites. For this reason, it is advantageous to use a metal matrix without any surface modification of LDO particles reinforced.

The microindentation technique is widely used for the determination of the mechanical properties of various materials, including the hardness of electrolytically deposited coatings. A number of studies investigated different experimental approaches for the determination of mechanical properties using continuous or discontinuous indentations in order to assess hardness, elastic modulus, toughness [31–33], and indentation creep [27,28,34]. Unlike continuous methods, where the curves are automatically recorded, the discontinuous method works on the principle of a determination of hardness point by point by applying various loads. In this case, in order to avoid the effect of substrate, it is necessary to apply small loads or to use different composite hardness models to eliminate the contribution of substrate to measured composite hardness [27,28,34]. The discontinuous Vickers approach is used for an estimation of the intrinsic (absolute; true) hardness of a wide range of materials, such as metals (including pure metal and metal matrix coatings), ceramics, and thermoplastic polymers [35,36].

The application of LDH/LDO nanoparticles in co-deposition mechanisms with metal ions from acidic electrolytes, especially as reinforcement in metal matrices, has not been extensively studied yet. This work aims to explore the functional properties of the copper matrix that served as the basic material for the incorporation of nanoparticle reinforcement based on Fe/Al LDO. As co-deposition is conducted in an acidic sulphate electrolyte, LDH particles are unsuitable, requiring conversion into a more stable layered double oxide (LDO) phase. Following this idea, this research comprised several components: the synthesis and characterization of Fe/Al LDO nanoparticles, stability testing of Fe/Al LDO particles in an acidic sulphate electrolyte, co-electrodeposition of Fe/Al LDO particles in a copper matrix, and characterization of the resulting composite coatings. Microstructural, topographical, textural, and mechanical (hardness) analyses, along with coating wetting, are crucial for the coating's further utilization, and they were analyzed.

2. Materials and Methods

2.1. Materials and Synthesis of Fe/Al LDH/LDO Nanoparticles

The synthesis of Fe/Al LDH is the initial step in the synthesis of Fe/Al LDO. Fe/Al LDH particles (molar ratio Fe:Al = 3:1) were synthesized from an aqueous solution under ambient conditions using the coprecipitation technique. Separately, $FeCl_2 \cdot 4H_2O$ (0.015 mol) and $Al_2(OH)_5Cl_2 \cdot 2.5\ H_2O$ (0.005 mol) were dissolved in 100 mL of deionized water. Drop by drop, 1 mol/L NaOH was added to the solution until the pH reached 10, at which point the addition was terminated. After allowing the dispersion to stand for 24 h, it was centrifuged at 6000 rpm for 10 min. Water was then used to wash the particles until the pH of the effluent solution was neutral. To obtain Fe/Al LDH particles, the material was dried with filter paper at 80 °C for 24 h. The produced Fe/Al LDH particles were then heated at 600 °C in the oven for 3 h. In this way, LDH is converted to LDO.

2.2. Materials for Cu and Cu-Fe/Al LDO Coating Preparation

Pure copper foil, 1.0 mm thick (99.99%) and brass foil ASTM B36 (70% Zn and 30% Cu), 250 μm thick, were used as anode and cathode, respectively. The copper foil was purchased from Alfa Aesar ThermoFisher GmbH Erlenbachweg, Kandel, Germany, and the brass foil from K and S Engineering, Chicago, IL, USA. Copper (II)-sulphate pentahydrate ($CuSO_4 \cdot 5H_2O$) and sulphuric acid (98%) of p.a. quality were ordered from Sigma-Aldrich (St. Louis, MO, USA). The high-purity water (Milipore, 18 MΩ·cm, Burlington, MA, USA) was used for the preparation of the electroplating baths.

2.3. Electrodeposition of Cu Coatings and Co-Electrodeposition of Cu/Fe-Al LDO Composite Coatings

Electrodeposition of copper coatings on the brass substrate was performed in an open cell (cylindrical Pyrex glass, 100 mL) under room conditions. The preparation of the brass

cathode is described in references [12,34]. The cathodes with a surface area of (2.0 × 1.0) cm^2 were positioned in the center of the electrolytic cell. The magnetic stirrer was used for the mixing of the electrolyte at 300 rpm. The basic sulphate electrolyte composition of 240 g/L $CuSO_4 \cdot 5\ H_2O$ and 60 g/L H_2SO_4 was used for electrodeposition of Cu coatings, and this electrolyte is notated as electrolyte BSE (Basic Sulphate Electrolyte). Electrodeposition of a 10 μm thick copper coating was performed in a direct current (DC) regime, assisted by magnetic mixing.

Co-electrodeposition was performed by the addition of 0.3 wt.% Fe/Al LDO nanoparticles into the BSE electrolyte, and these electrolytes were noted as BSE/LDO electrolytes. The BSE/LDO electrolyte was stirred for 90 min prior to the co-electrodeposition process, with the aim of better wetting of Fe/Al LDO nanoparticles by the electrolyte, suppression of their agglomeration, and better distribution of the nanoparticles in the volume of the electrolyte. The current density value was identical with both, without and with added Fe/Al LDO nanoparticles (j = 50 $mA \cdot cm^{-2}$). The thicknesses of the coatings with co-deposited Fe/Al LDO nanoparticles were 5, 10, 20, and 50 μm.

2.4. Preparation of Cross-Section for SEM/Mapping Analyses

The process of revealing the cross-section structure starts with a cut (perpendicular) of the coatings based on pure copper and those with incorporated Fe/Al LDO nanoparticles. The cutting samples with different thicknesses of coatings were embedded in a self-curing methyl methacrylate polymer (Veracril-Self-cure Acrylic) and mechanically polished with different SiC papers (#800, #1200, and #1500). The self-polymerization of the prepared sample took about 3–10 min, depending on the room temperature, in a Teflon mold. Before SEM/mapping analyses, to achieve better surface conductivity, a thin layer of gold was deposited over the acrylate sample.

2.5. Characterization Methods

Microstructural properties, texture, and roughness analyses were determined using a field emission scanning electron microscope (FE-SEM), an X-ray powder diffractometer (XRD), an optical microscope (OM), and an atomic force microscope (AFM). Image analysis was used for the particle size measurement and grain size distribution. The software enables us to identify and measure the size of the particles in the recorded surface morphology. In this study, image analysis was applied to FE-SEM micrographs representing the morphologies of pure Cu and Cu coatings with incorporated nanoparticles. The microhardness property of coatings was investigated using a Vickers indentation hardness tester. Characterization methods and settings are detailed and described in Supplementary Materials.

3. Results

3.1. Characterization of Fe/Al LDO Particles

3.1.1. Morphology of the Fe/Al LDO Particles

The morphology of the Fe/Al LDO particles synthesized in lab conditions using the co-precipitation method in order to use them as reinforcements in the copper matrix composites is shown in Figure 1a, while the distribution of particle diameters is given in Figure 1b. The morphology of Fe/Al LDO particles is well kept in spherical shapes, and they have nanodimensions. More precisely, Fe/Al LDO shows a diameter of 5–65 nm (Figure 1b), with slightly smaller Fe/Al LDO nanoparticles attached to a bigger agglomerated form and a more distinct spherical contour, probably due to the removal of interlayer water molecules after calcination [37]. The nano-scaled particles of LDOs tend to agglomerate in the form of bigger particles or micro-sheets (Figure 1a) due to the strong particle–particle interactions, indicating that electrolyte mixing must be applied during co-deposition. The average size of Fe/Al LDO particles was about 17 nm (Figure 1b).

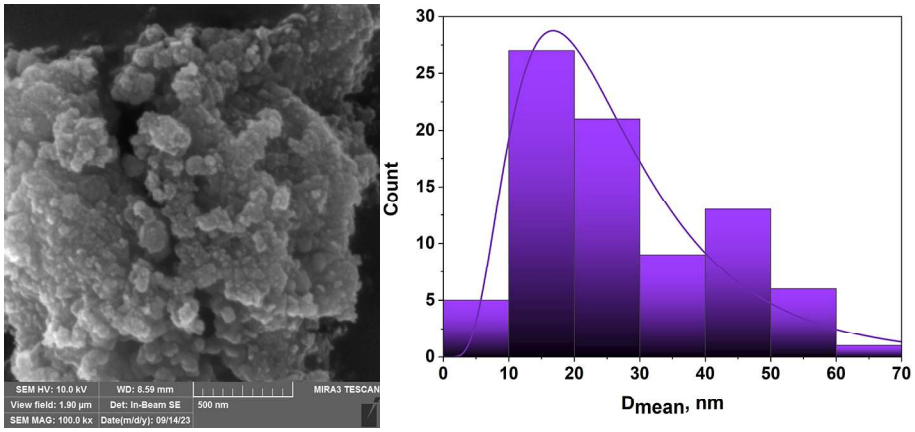

Figure 1. (**a**) FE-SEM micrograph of Fe-Al LDO, and (**b**) distribution observed particle diameters.

3.1.2. The XRD Analysis of the Fe/Al LDO Particles

The XRD patterns of Fe/Al LDH and Fe/Al LDO particles obtained after calcinations of Fe/Al LDH are given in Figure 2. The peaks observed in the XRD data from Figure 2a are indicative of the LDH structure. Specifically, the diffraction peaks at 11.7°, 23.7°, 39.4°, and 63.1° are characteristic of the typical layered structure of LDH. These findings from XRD data demonstrate the successful transformation of $FeCl_2$ and aluminium hloralhydrate into the LDH phase, as supported by previous studies [38]. According to XRD data (Figure 2b), the Fe/Al LDO sample consists of ceramic and metal components. The main oxide phases are hematite (JSPDS 00-071-0073) and maghemite (JSPDS 00-004-0755), while corundum (JSPDS 00-001-1296), magnetite (JSPDS 00-001-1111), and spinel $FeAl_2O_4$ (JSPDS 01-082-3023) are minor phases [39].

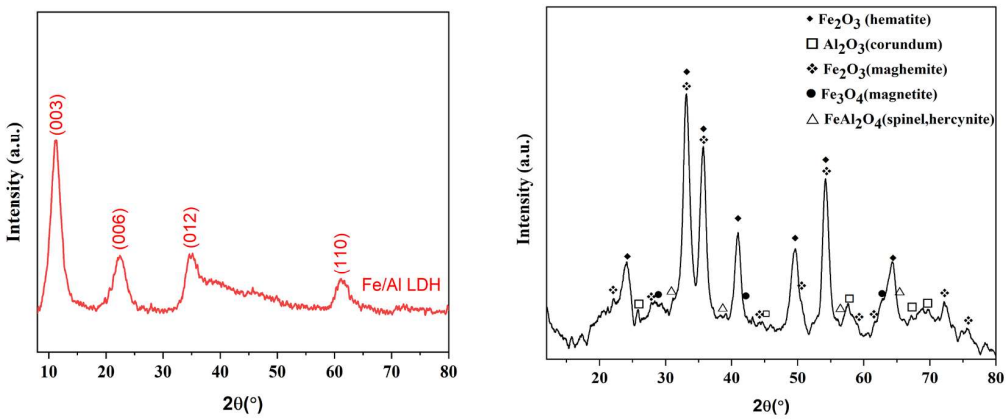

Figure 2. The XRD patterns of: (**a**) Fe/Al LDH particles and (**b**) Fe/Al LDO particles.

3.1.3. Morphology of the Suspension of BSE/LDO Electrolyte after Evaporation

The features of Fe/Al LDO nanoparticles in extremely acidic electrolytes were observed through the microstructure of the electrolyte precipitate after water evaporation (Figure 3). This research was carried out to observe possible changes in the microstructure of Fe/Al LDO particles under extremely acidic medium conditions. The intact structure of the Fe/Al LDO particle form was observed by detecting the BSE/LDO electrolyte precipitate.

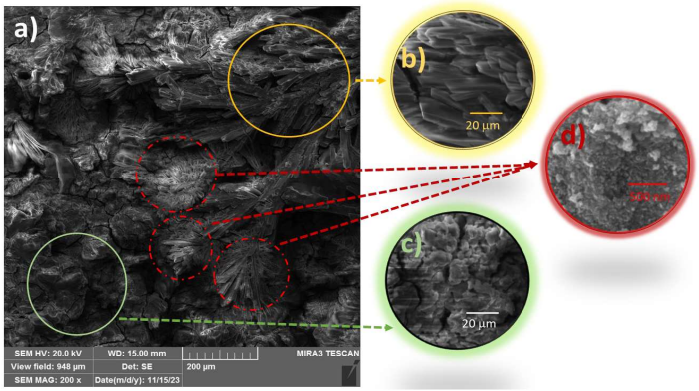

Figure 3. FE-SEM micrographs of evaporated BSE/LDO electrolyte on Al foil obtained on variation of magnification: (**a**) ×200, and with magnified characteristic details: (**b**,**c**) ×2000, and (**d**) ×100,000.

The microstructure of the precipitate observed at higher magnifications is shown in Figure 3b–d. Figure 3a shows the microstructures of the precipitate of BSE-LDO electrolyte after evaporation, and three different microstructural forms are noticed: micro-sheets (Figure 3b), micro-flakes (Figure 3c), and nano-spheres (Figure 3d). It follows from the analysis of BSE-LDO electrolyte sediment that specific microstructures are formed without microstructural changes in spherical forms of LDO nanoparticles (Figures 1a and 3d). Figure 3b shows micro-sheets that are formed from elemental sulphur, known as "flowers of sulphur" [40], and that are confirmed by elemental analysis and mapping (Figure 4).

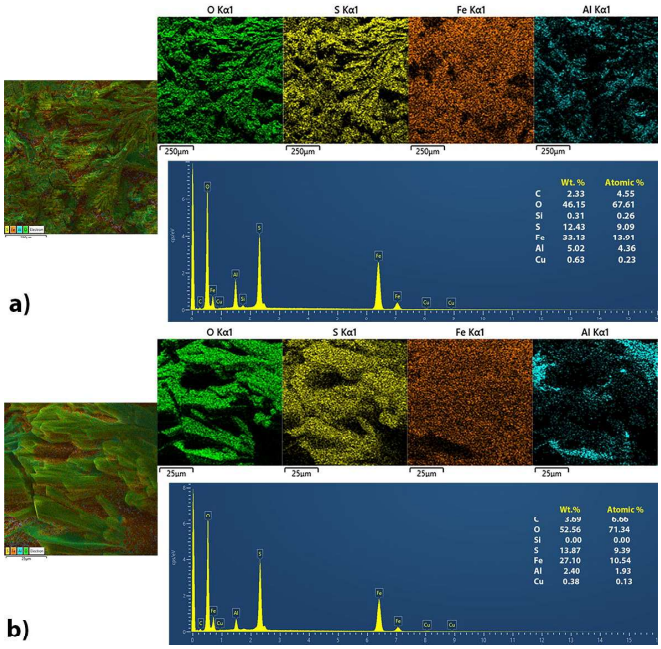

Figure 4. FE-SEM micrographs of evaporated BSE/LDO electrolyte on Al foil with mapping and an EDS spectrum obtained on different locations from: (**a**) Figure 3c, and (**b**) Figure 3b.

3.1.4. Elemental Analysis Suspension of BSE/LDO Electrolyte after Evaporation

The microstructural stability of the suspension of BSE electrolyte in the presence of LDO particles (Al^{3+}, Fe^{2+} ions) was evaluated using the elemental mapping shown in Figure 4. Figure 4 presents characteristic locations from Figure 3b,c, which were characterized using EDS/mapping in order to indicate the composition of the suspension after the evaporation of BSE/LDO electrolyte on aluminum foil. The elemental mapping image analysis displayed that the suspension was composed of S, Fe, Al, O, C, Si, and Cu. It is clear from Figure 4 that Fe and Al are evenly distributed and present at the edges and flat

parts of microstructural forms, while oxide and sulphur forms dominate on sharp parts. If we take into account that the co-deposition of LDO particles in the copper matrix takes place in an acidic sulphate electrolyte, it was necessary to examine the behavior (stability) of these particles in the BSE electrolyte. Examining the chemical content and microstructure of the precipitate of BSE/LDO electrolyte, it is clear that the oxide particles are inert in the acidic electrolyte and that no degradation occurred (Figures 3 and 4).

3.2. Characterization of Copper and Cu-Fe/Al LDO Composite Coatings

The effect of Fe/Al LDO nanoparticles as reinforcement on the morphology, texture, hardness, and wettability of electrolytically deposited Cu coatings was examined by the analysis of Cu coatings of various thicknesses obtained with the constant concentration of these nanoparticles. For a clearer analysis of the effect of this reinforcement on the above-mentioned characteristics of the Cu coatings, a 10 μm thick coating was compared with that obtained from the basic sulphate electrolyte (without Fe/Al LDO nanoparticles). In the future text, Cu coatings obtained from the basic sulphate electrolyte are denoted as pure Cu coatings, while those obtained with the incorporation of Fe/Al LDO nanoparticles are called Cu-Fe/Al LDO coatings.

3.2.1. Morphological Analysis of the Pure Cu and Cu-Fe/Al LDO Coatings; FE-SEM Analysis

Figure 5 shows surface morphologies of the 10 μm thick pure Cu coating (Figure 5a) and Cu-Fe/Al LDO coatings (Figure 5b–e) electrodeposited with a concentration of Fe/Al LDO nanoparticles of 0.3 wt.% with varying coating thicknesses in the range of 5–50 μm. The appropriate histograms of grain size distribution obtained by an image analysis of FE-SEM micrographs are also given in Figure 5.

The difference between the pure Cu coating and the Cu-Fe/Al LDO coatings with a variation in thickness is only reflected in the size and the distribution of grains, while morphologically, no difference was observed. All Cu coatings are compact and microcrystalline. A boundary between the grains is clearly visible, and based on the grain size distribution histograms, the average grain size (D_{mean}) for each formed coating was estimated and given in Table 1. The minimal grain size had a 5 μm thick Cu coating with Fe/Al LDO nanoparticles (0.78 μm), and grain size increased with the deposition time, i.e., with a coating thickness up to 3.02 μm for the 50 μm thick Cu-Fe/Al LDO coating. A comparison of coatings without and with Fe/Al LDO nanoparticles of the same thickness (10 μm) indicates that the presence of Fe/Al LDO nanoparticles increases the grain size of the copper coatings by about 60%.

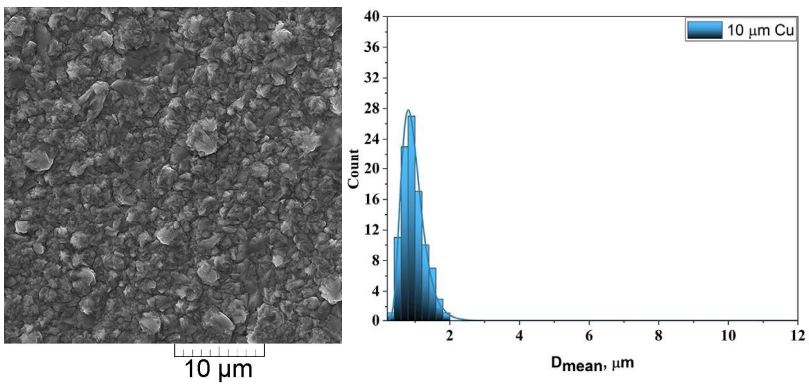

(**a**)

Figure 5. *Cont.*

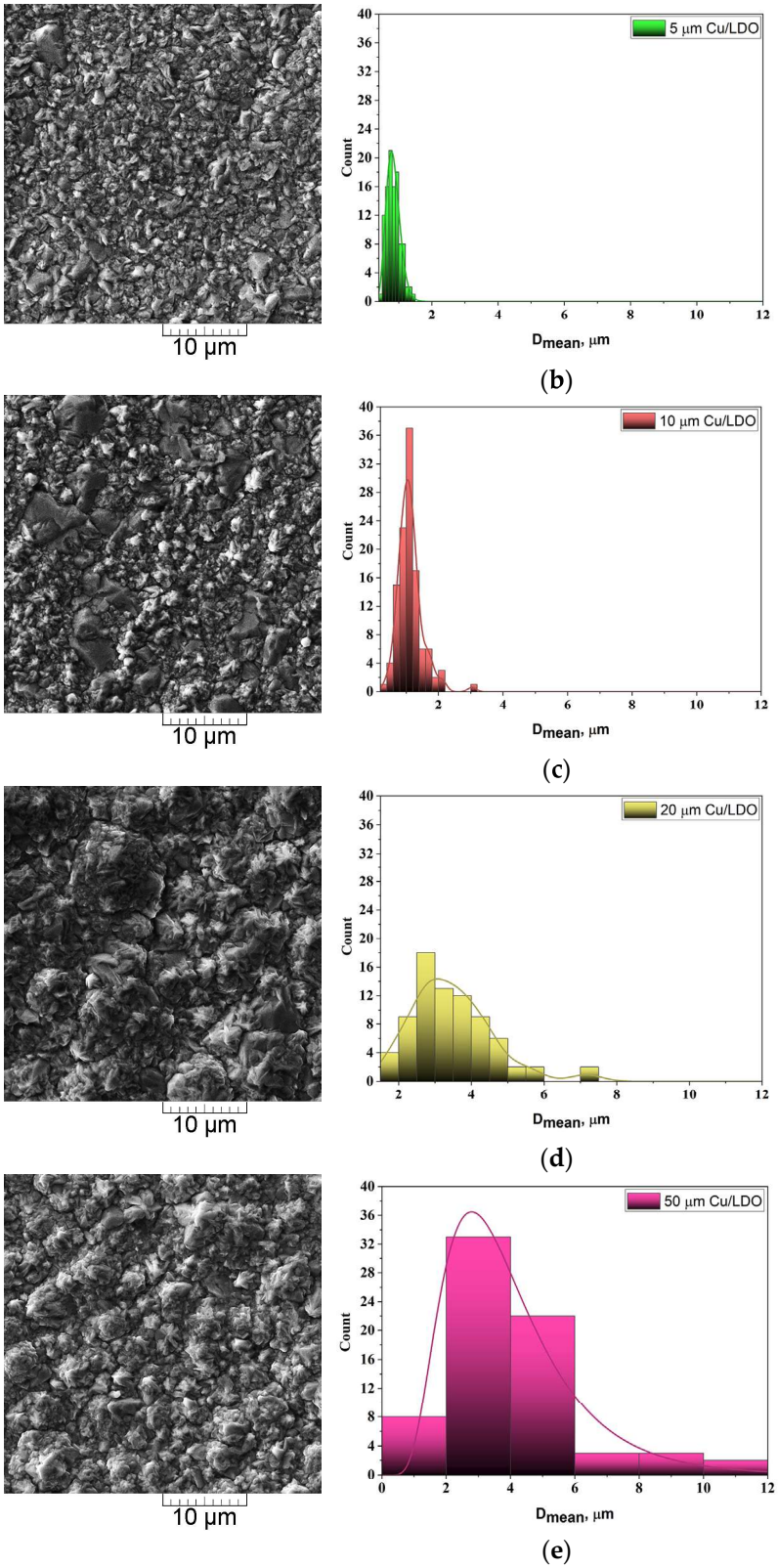

Figure 5. FE-SEM micrographs of Cu: (**a**) 10 µm Cu and Cu-Fe/Al LDO coatings: (**b**) 5 µm, (**c**) 10 µm, (**d**) 20 µm, and (**e**) 50 µm with appropriate histograms of grain size distribution. The magnification was ×5000.

Table 1. The estimated average grain size distribution obtained from FE-SEM images.

Sample No.	Electrolyte	Experimental Thickness of Coatings, δ (µm)	Grain Size, D_{mean} (µm)
1.	BSE/LDO	5	0.80
2.	BSE	10	0.78
3.	BSE/LDO	10	1.25
4.	BSE/LDO	20	2.85
5.	BSE/LDO	50	3.02

Mapping/EDS Analysis of the Pure Cu and Cu-Fe/Al LDO Coatings

Figure 6 shows the mapping analysis of the pure Cu coating electrodeposited from the BSE electrolyte thickness of 10 µm (Figure 6a) with the elemental distribution of Cu (green dots) and O (red dots). The EDS spectrum was given in Figure 6b, and the presence of copper was confirmed in the percent (99.5 wt.% or 98.19 atomic%). The traces of native oxide formed on the coating surface were also detected (0.5 wt.% or 1.81 atomic%).

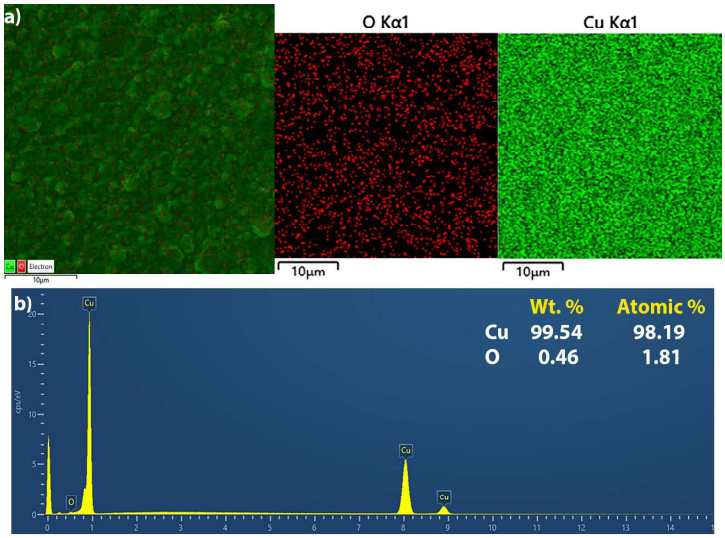

Figure 6. An element mapping of the pure Cu coating (10 µm thick) electrodeposited from the BSE electrolyte: (**a**) mapping and (**b**) an EDS spectrum.

Figure 7 represents the mapping analysis of the coating of the same thickness of 10 µm electrodeposited with Fe/Al LDO nanoparticles. The elemental distribution on the surface of a 10 µm thick Cu-Fe/Al LDO coating showed the presence of the following elements: Cu (74.2%), Fe (0.07%), Al (0.30%), O (2.12%), and C (23.3%). The amount of Fe/Al LDO particles on the coating surface is expected to be low because the particles are deeply incorporated into the interior of the coating [12]. However, the proportion of carbon and oxygen in this coating is higher compared to a pure copper coating. This indicates an increased absorption power of the composite coating and a slightly more porous structure, so that the retention of oxygen and carbon is increased [41].

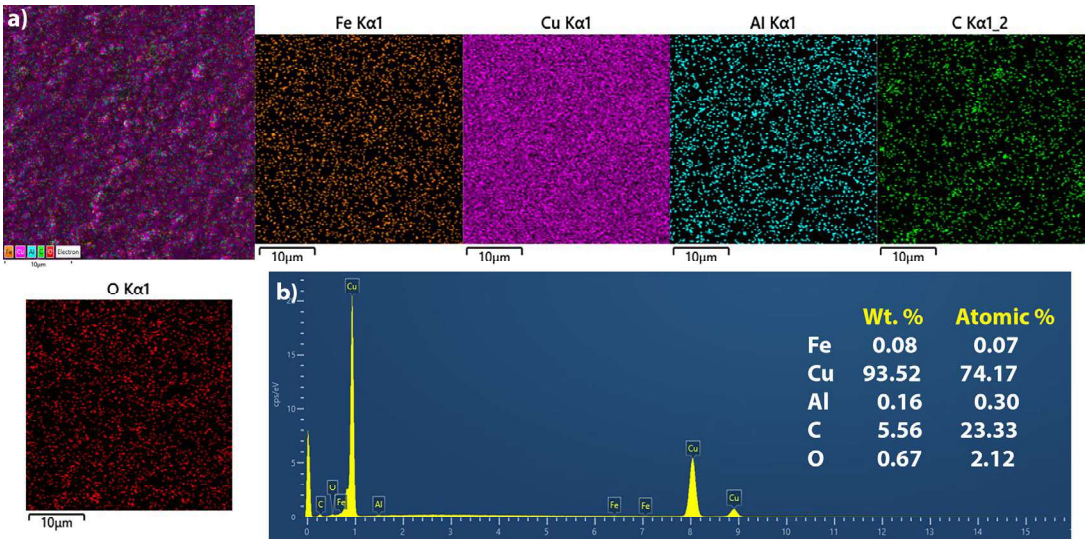

Figure 7. Element mapping of the Cu-Fe/Al LDO coating (10 µm thick) electrodeposited from the BSE electrolyte with an addition of 0.3 wt.% of Fe/Al LDO particles: (**a**) mapping and (**b**) an EDS spectrum.

The Cross-Section Analysis of Cu-Fe/Al LDO Composite Coatings

The cross-sections of Cu-Fe/Al LDO coatings and the elemental mapping image analysis of all thicknesses were also performed (Figure 8). A large percentage of zinc comes from the substrate (brass B36). According to the cross-sections, it follows that the thickness of Cu coatings was in agreement with theoretical predictions.

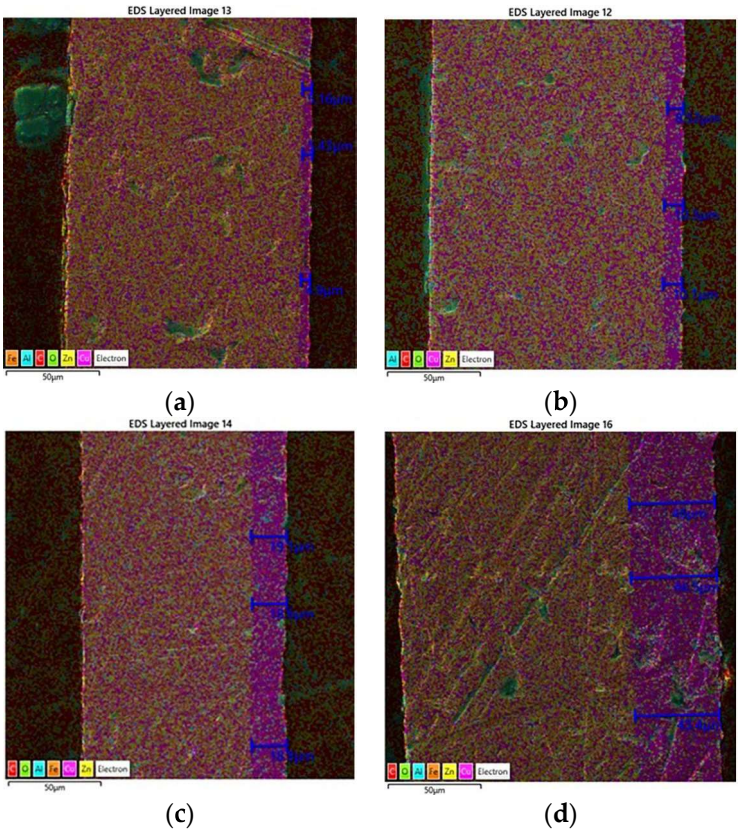

Figure 8. Elemental mapping analyses performed on the cross-sections of the Cu-Fe/Al LDO coatings obtained with 0.3 wt.% of Fe/Al LDO nanoparticles added in the BSE electrolyte: (**a**) 5 µm, (**b**) 10 µm, (**c**) 20 µm, and (**d**) 50 µm.

3.2.2. Topographical Analysis of the Pure Cu and Cu-Fe/Al LDO Coatings—AFM Analysis

Figure 9 shows the topography and the corresponding histograms of the coatings obtained without (Figure 9a) and with the Fe/Al LDO nanoparticles as reinforcement (Figure 9b–e). The values of an arithmetic average of the absolute roughness parameters (R_a) were 152.5 nm for the coating obtained from the BSE electrolyte and 194.6 nm for the coating of the same thickness obtained from the BSE/LDO electrolyte, which indicates the existence of a strong roughness effect (21.6%) of the Fe/Al LDO nanoparticles (see Table 2). The increase in roughness of the Cu-Fe/Al LDO coatings is a result of both the roughening of the electrode surface with the electrodeposition time and the incorporation of Fe/Al LDO nanoparticles in the coatings. This increase in non-uniformity of Cu coatings is also accompanied by an increase in the size of the grains, as indicated by Figure 5. It is in agreement with the basic laws of electrocrystallization, where the rise in both roughness and size of grains is expected with increasing the electrodeposition time [42]. This effect was enhanced by the incorporation of hard nanoparticles in the coatings. Comparing 5 μm and 50 μm thick Cu-Fe/Al coatings, it is obvious that the difference in roughness was 68.82%.

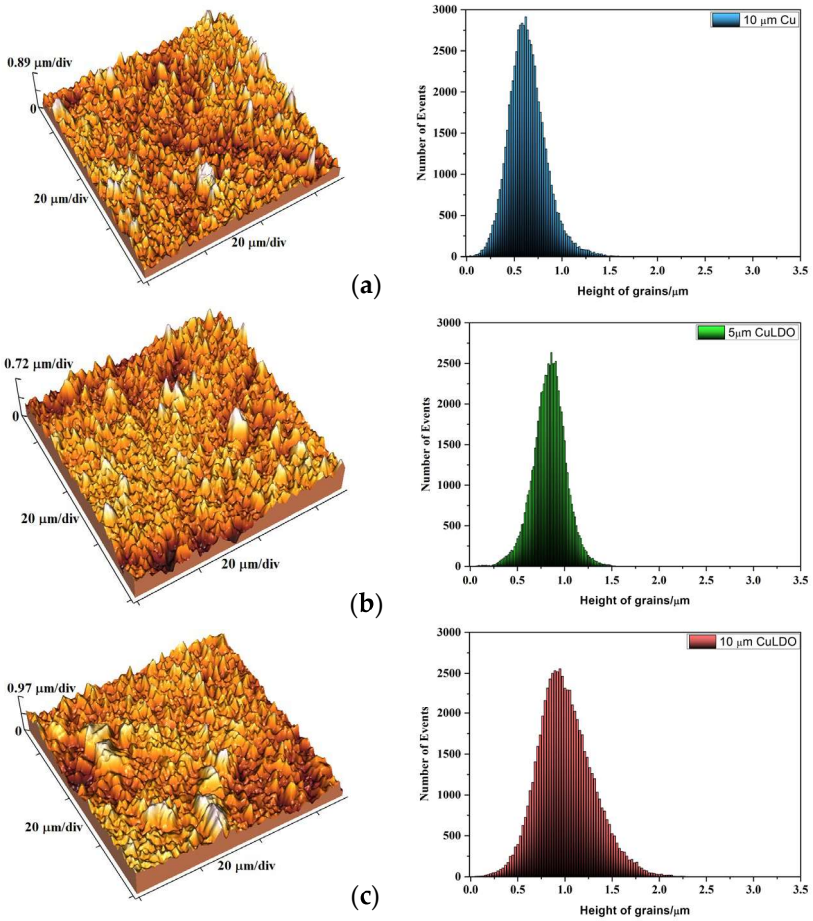

Figure 9. *Cont.*

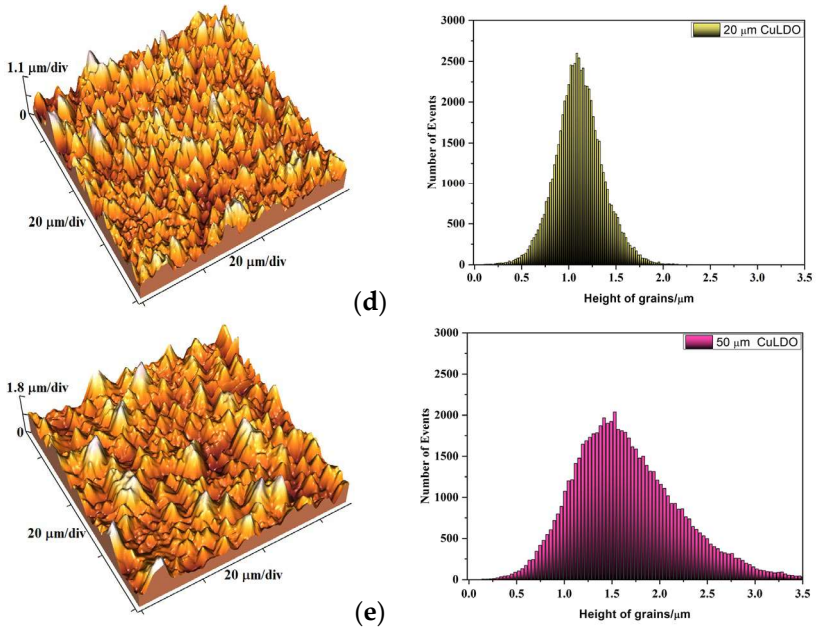

Figure 9. The three-dimensional AFM images and the corresponding histograms of the pure Cu and Cu-Fe/Al LDO coatings obtained with variations in thickness: (**a**) 10 μm pure Cu coating, and Cu-Fe/Al LDO coatings with a thickness of: (**b**) 5 μm, (**c**) 10 μm, (**d**) 20 μm, and (**e**) 50 μm. AFM surface scan size was (70 × 70) μm^2.

Table 2. The values of the roughness parameter (an arithmetic average of the absolute roughness (R_a) and the average height of grains (h_{av})) obtained by application of AFM software from (70 × 70) μm^2 scan area for the pure Cu and Cu-Fe/Al LDO coatings.

δ (μm)/Coating Types	10 μm/ Cu	5 μm/Cu-Fe/ Al LDO	10 μm/Cu-Fe/ Al LDO	20 μm/Cu-Fe/ Al LDO	50 μm/Cu-Fe/ Al LDO
R_a (nm)	152.5	136.9	194.6	231.3	439.1
h_{av} (nm)	648.8	846.5	1022.1	1121.7	1675.8

3.2.3. Textural Analysis (XRD) of the Copper and Cu-Fe/Al LDO Coatings

The X-ray diffraction (XRD) patterns of the pure Cu and Cu-Fe/Al LDO coatings are shown in Figure 10. The diffraction peaks at 2θ angles of 43.3°, 50.4°, 74.1°, and 89.9° correspond to (111), (200), (220), and (311) crystal faces of the face-centered cubic (FCC) crystal lattice of Cu (JSPDS 04-0836) [43]. Aside from the peaks of metallic Cu, small peaks originating from two copper oxides (Cu_2O and CuO) were also detected. The first small peak at 42.32° corresponds to the (200) crystal plane of the cubic structure of Cu_2O (JCPDS#01-077-0199) [44], while the diffraction peaks at 2θ angles of 42.32°, 49.23°, 72.22°, and 87.41° correspond to the (111), (−202), (−311) and (−223) crystal planes of the monoclinic form of copper oxide, tenorite (JCPDS#01-080-0076) [45]. The appearance of oxides is probably a consequence of inadequate treatment of the Cu coatings after the completed process of electrochemical deposition and is not influenced by the addition of Fe/Al LDO nanoparticles. The proof for this statement can be found in the absence of oxide peaks in the thicker coatings, as well as in their appearance in the Fe/Al LDO-free Cu coating. Certainly, the corresponding crystalline planes related to Fe/Al LDO were not detected in these patterns, probably due to the low concentration of Fe/Al LDO in the coatings, as already considered for the Cu coatings obtained with the pigment particles based on strontium aluminate [12].

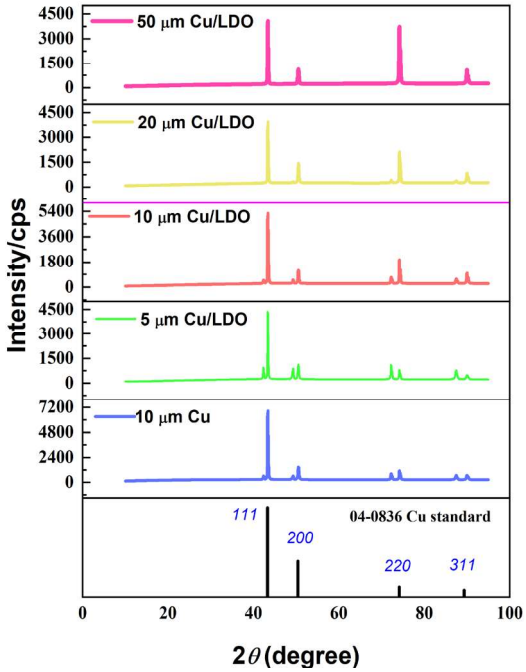

Figure 10. The XRD patterns for the pure Cu and Cu-Fe/Al LDO coatings electrodeposited/co-electrodeposited in the DC/MS regime on the brass substrate with a variation of coating thickness in the (5–50 μm) range.

It is necessary to note that increasing the coating thickness increases the share of Cu crystallites oriented in the (220) crystal plane. The texture, i.e., the preferred orientation of Cu coatings, was determined by a determination of the texture coefficients. The calculated values of "texture coefficient", *TC*(*hkl*), and "relative texture coefficient" *RTC*(*hkl*), [12,43] are presented in Table 3, while a description of the procedure for a determination of these coefficients is given in Supplementary Materials. The values of *TC* coefficients larger than 1 and the *RTC* coefficients larger than 25% (four main Cu reflections were analyzed) point out the existence of the preferred orientation [12,43].

Table 3. The values of *TC*(*hkl*) and *RTC*(*hkl*) coefficients calculated for the pure Cu and Cu-Fe/Al LDO coatings with variations in the thickness.

Electrolyte	δ/μm	*TC*(*hkl*)				*RTC*(*hkl*)/%			
		TC(*111*)	*TC*(*200*)	*TC*(*220*)	*TC*(*311*)	*RTC*(*111*)	*RTC*(*200*)	*RTC*(*220*)	*RTC*(*311*)
BSE	10	1.24	0.59	1.02	0.69	35.0	16.7	28.8	19.5
BSE/LDO	5	1.18	0.66	1.08	0.77	32.0	17.9	29.3	20.8
BSE/LDO	10	1.02	0.50	1.94	1.12	22.3	10.9	42.4	24.4
BSE/LDO	20	0.86	0.68	2.34	1.08	17.3	13.7	47.2	21.8
BSE/LDO	50	0.75	0.45	3.42	1.14	13.0	7.80	59.4	19.8

From Table 3, it can be seen that the pure Cu coating and the 5 μm thick Cu-Fe/Al LDO coating possess the (111)(220) preferred orientation. However, the Cu-Fe/Al LDO coating thicknesses of 10, 20, and 50 μm exhibited the (220) preferred orientation, whereby the degree of this preferred orientation increased with increasing the coating thickness.

It is clear that this change in the preferred orientation cannot only be attributed to the increase in coating thickness but also to the addition of Fe/Al LDO nanoparticles, since 10 μm thick Cu coatings obtained without/with Fe/Al LDO nanoparticles exhibited various preferred orientations.

It can be observed that the average crystallite size of the copper coatings is about 30 nm (Figure 11) and that the incorporation of Fe/AL LDO nanoparticles in the copper matrix did not drastically influence the values of the average crystallite size. With the increase in the thickness of the nanoparticle-reinforced coatings, a slight decrease in the crystallite size was observed, from 29.44 nm for the coating with a thickness of 5 μm to 25.83 nm for the coating with a thickness of 50 μm.

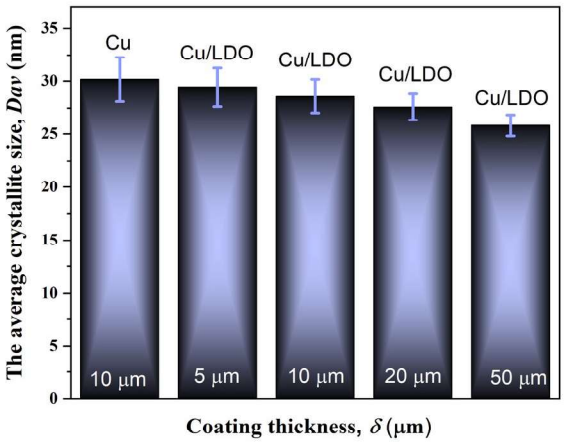

Figure 11. The values of an average crystallite size for the pure Cu and Cu/Fe/Al LDO coatings were determined from the XRD data using the Debye-Scherrer formula.

3.2.4. Analyses of Microhardness Features of the Pure Cu and Cu-Fe/Al LDO Coatings

An intrinsic (true, absolute) hardness of pure Cu and Cu-Fe/Al LDO coatings was determined by an application of the Chicot-Lesage (C-L) composite hardness model (C-L CHM) [12,34,45–50]. This model proved to be very successful in estimating the intrinsic hardness of thicker copper coatings [34,45], as well as for copper coatings reinforced with ceramic microparticles [12]. A detailed description of the C-L model is presented in the previous studies [45–50]. In order to better perceive the effect of Fe/Al LDO nanoparticles on the coating hardness, the hardness of the coatings obtained with the reinforcement in the (5–50) μm thickness range was compared with the 10 μm thick Cu coating obtained from the reinforcement-free electrolyte.

Figure 12a,b illustrate the dependence of the composite hardness (H_c) measurements on the relative indentation depth (RID) for the 10 μm thick Cu coatings electrodeposited from the BSE and the BSE/LDO electrolytes (Figure 12a) and those thicknesses of 5, 20, and 50 μm obtained from the BSE/LDO electrolyte (Figure 12b). The dependence of the intrinsic hardness (H_i) calculated according to the C-L CHM on RID for the same coatings are shown in Figures 12c and 12d, respectively. The RID is expressed in the form RID = h/δ, where h is the depth of Vickers's indentation and δ is the coating thickness [45]. A diagonal size, d, and Vickers's indentation depth are connected by the formula $h = d/7$, and this connection arises from the geometry of the pyramid indenter [45].

The exponential dependence of the $(\delta/d)^m$ on the RID for the analyzed Cu and Cu-Fe/AL LDO coatings is shown in Figures 12e and 12f, respectively. It is necessary to note that the critical RID value of 0.14 obtained by hypothesizing the validity of C-L CHM up to $(\delta/d)^m = 1$ is denoted in Figure 12e,f. For the sake of easier analysis of this composite hardness system, the native H_c and calculated H_i values are also given in Table S1 in Supplementary Materials.

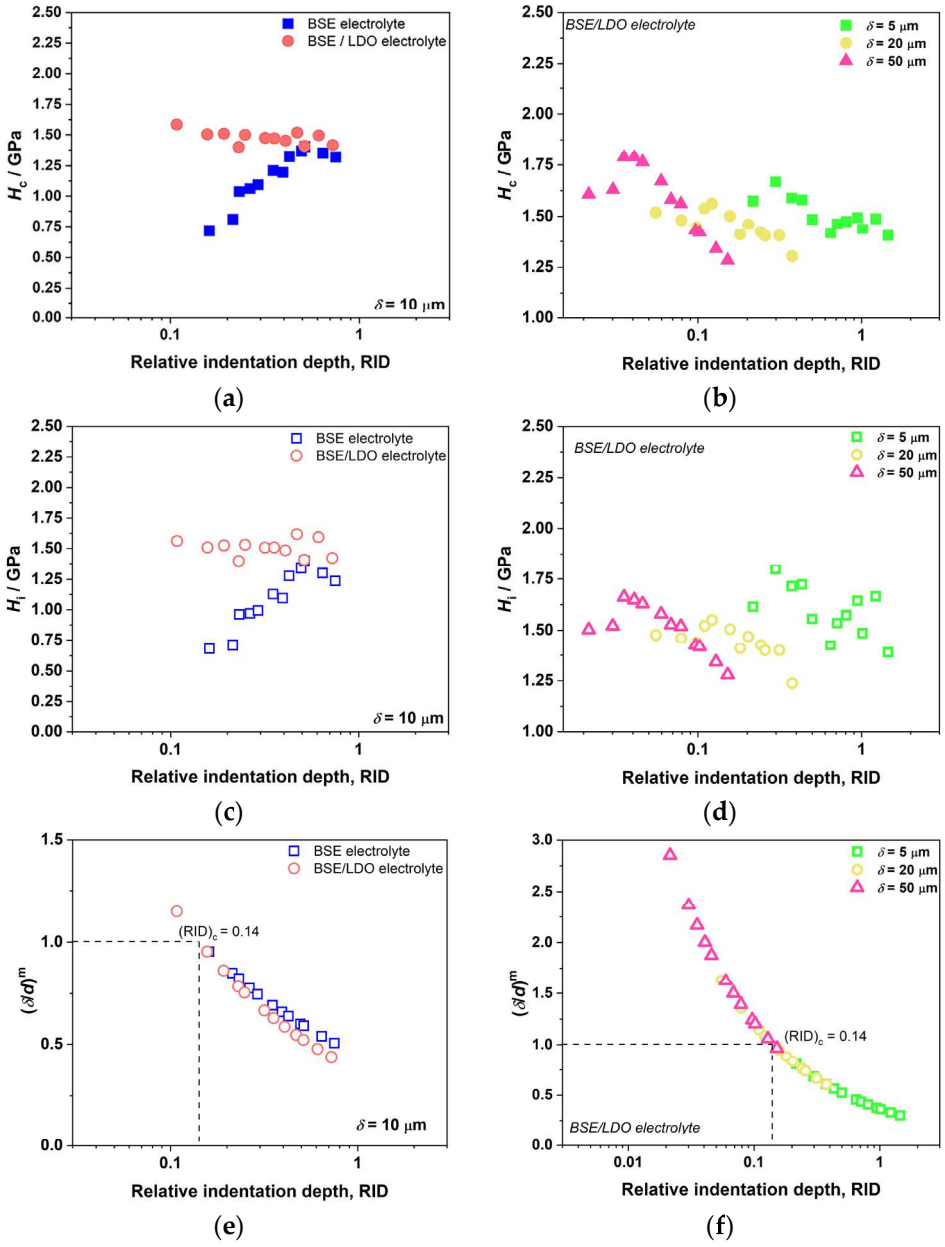

Figure 12. The dependencies of: (**a**) H_c on RID for 10 μm thick Cu coatings obtained without and with Fe/Al LDO; (**b**) H_c on RID for 5, 20, and 50 μm thick Cu coatings obtained with Fe/Al LDO; (**c**) H_i on RID for 10 μm thick Cu coatings obtained without and with Fe/Al LDO; (**d**) H_i on RID for 5, 20, and 50 μm thick Cu coatings obtained with Fe/Al LDO. The dependencies of $(\delta/d)^m$ on RID for: (**e**) 10 μm thick Cu coatings obtained without and with Fe/Al LDO and (**f**) 5, 20, and 50 μm thick Cu coatings obtained with Fe/Al LDO.

In order to determine the intrinsic hardness of Cu and Cu-Fe/Al LDO coatings using the C-L CHM, knowledge of both the hardness of the cathode (substrate) and a parameter called Meyer's composite index, *m*, which is computed for each coating individually, is necessary [12,34,45–52]. Meyer's composite index, denoted as (*m*), quantifies the relationship between the microhardness of a composite and the size of an indentation. The values of the composite Meyers' index and coefficient of determination (R^2) for Cu and Cu-Fe/Al LDO coatings are shown in Figure 13, while a calculated substrate hardness value was 1.41 GPa [12,34,45].

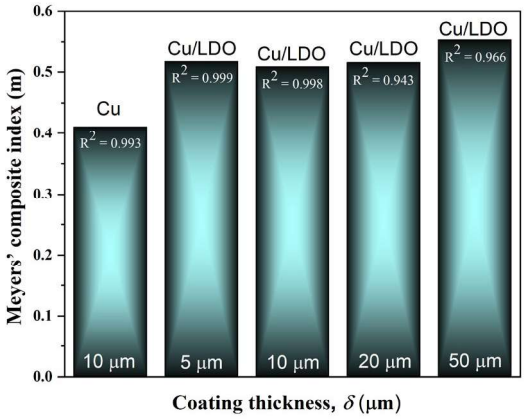

Figure 13. The values of Meyers' composite index for the pure Cu and Cu/Fe/Al LDO coatings with variation of thickness.

Application of the C-L CHM in an analysis of the hardness of Cu coatings identified the critical RID value of 0.14, which separated two zones: zone (I)—for RID < 0.14 where the measured composite coating hardness matches its hardness (in this zone $H_c < H_i$), and zone (II)—for $(RID)_c \geq 0.14$ in which the C-L CHM must be applied to obtain an intrinsic coating hardness (in this zone $H_c > H_i$) [12,45]. This is valid for "soft film on hard cathode" systems, such as electrodeposited Cu coatings from the BSE electrolyte by the DC and by the pulsating current (PC) regimes [43,45], as well as from the BSE electrolyte with added levelling/brightening additives [50]. Recently, the opposite behavior left and right from the 0.14 critical RID value from above-mentioned was observed for the Cu coatings reinforced with micro-sized particles based on strontium-aluminate [12]. Based on this opposite behavior, it was concluded that the addition of this particle type caused a transformation of the composite hardness system into a "hard film on soft cathode" kind.

It is evident from an analysis of 10 pure Cu coatings (Figure 12a) that the computed intrinsic hardness (H_i) values (Figure 12c) were significantly greater than the measured composite hardness (H_c) values for RID values lower than 0.14 ($(RID)_c < 0.14$). For $(RID)_c \geq 0.14$, H_i was smaller than H_c, and the calculated hardness values by C-L CHM represent the intrinsic coating hardness. In this way, it is clear that pure Cu coating behaves as "soft film on hard cathode".

The different shapes of the H_c on the RID dependencies for the Cu coatings with incorporated Fe/Al LDO nanoparticles (Figure 12a,b) clearly signified the change of the type of composite hardness system from "soft film on hard cathode" into "hard film on soft cathode" type. It is proved by an analysis of the H_i on the RID dependencies (Figure 12c,d) as well as the data given in Supplementary Materials (Table S1) for these coatings. Regarding the Cu coatings with incorporated Fe/Al LDO nanoparticles, the H_c values are larger than H_i for $(RID)_c < 0.14$ and the H_c values are smaller than H_i for $(RID)_c \geq 0.14$. In this way, it is confirmed that the addition of Fe/Al LDO nanoparticles in the BSE electrolyte caused a transformation from "soft film on hard cathode" to "hard film on soft cathode" systems.

Also, an additional analysis of Cu coating thickness from 5 μm was necessary. This coating was very thin, and for larger applied loads, i.e., RID values about and larger than 1, the composite hardness corresponds to the hardness of the cathode (substrate). It meant that the application of the larger loads was not appropriate for the thin coatings.

3.2.5. Analyses of Wettability Features of the Pure Cu and Cu-Fe/Al LDO Coatings

The static water contact angle (θ_c) is the angle at the interface where water, air, and solids meet [53]. Low contact-angle values mean the tendency of the droplet of water to adhere well to the surface ($\theta_c < 90^\circ \Rightarrow$ hydrophilic property), and very high wetting angle values indicate the hydrophobic properties ($\theta_c > 90^\circ$) of a coating [53,54]. The limiting contact angle for the transition from hydrophilicity to hydrophobicity is greater than

90° [12,53–57]. The appearance, shape of water droplets on coating, and measured contact angles for 10 μm LDO-free Cu coating and for those of various thicknesses obtained with Fe/Al LDO particles are given in Figure 14a–e. The obtained values of water contact angles are given on a histogram shown in Figure 14f. The copper coating obtained without Fe/Al LDO nanoparticles shows hydrophilic behavior ($\theta_c < 90°$), while those with incorporated Fe/Al nanoparticles thickness larger than 10 μm show the hydrophobic character. The hydrophilic/hydrophobic properties of the coatings, depending on the value of the water contact angle, are described in the Discussion section.

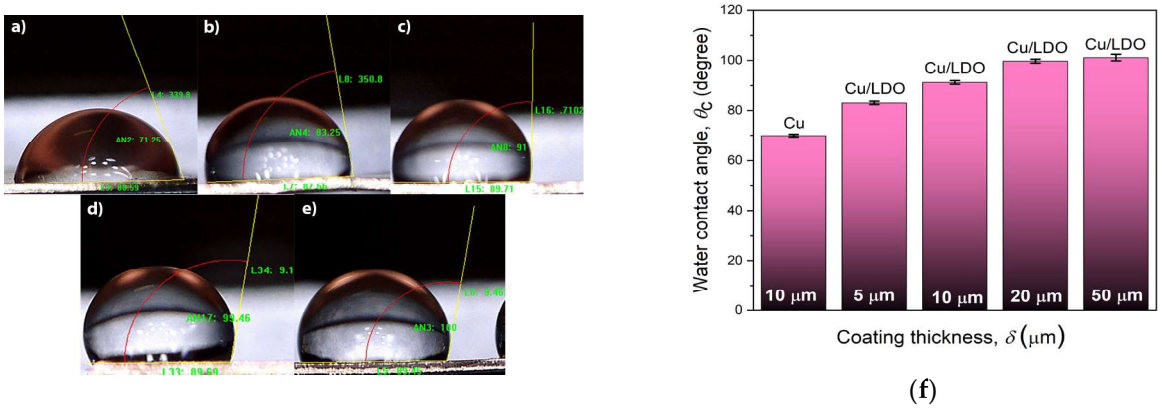

(**f**)

Figure 14. Wettability properties of Cu and Cu-Fe/Al LDO coatings on brass substrates: (**a**) water droplets on 10 μm pure Cu and on Cu-Fe/Al LDO coatings with variation in thickness: (**b**) 5 μm, (**c**) 10 μm, (**d**) 20 μm, (**e**) 50 μm, and (**f**) an appropriate histogram of water contact angles measured.

4. Discussion

Fe/Al LDO particles were obtained from coprecipitation synthesized Fe/AL LDH by calcination. Those particles were then incorporated into the copper matrix as reinforcement by electrodeposition. The electrolytically produced Cu coatings with incorporated nano-sized Fe/Al LDO particles in the (5–50) μm thickness range were compared to the pure Cu coating of 10 μm thickness. The difference in size and distribution of Cu grains was only observed among the coatings without/with Fe/Al LDO nanoparticles (Figure 5). Also, the presence of Fe/Al LDO particles was detected on the surface of the produced coatings (Figure 7), as well as on the cross-section (Figure 8), which indicated their successful co-electrodeposition.

Analysis of the AFM images (Figure 9b–e) and appropriate histograms obtained for the Cu-Fe/Al LDO coatings showed that the height of grains and roughness parameter (R_a) increased with increasing deposition time, i.e., with the coating thickness. Comparing the coatings of the same thickness, the Cu-Fe/Al LDO coating showed a larger roughness, which is a consequence of the incorporation of Fe/Al LDO nanoparticles in the Cu matrix.

The best way to perceive the effect of Fe/Al LDO nanoparticles on the texture of the Cu coatings was a comparison of pure Cu and Cu-Fe/Al LDO coatings of the same thickness. As already mentioned, they showed various preferred orientation: (111)(220) for pure Cu, and (220) for Cu-Fe/Al LDO coatings. Simultaneously, the degree of (220) preferred orientation for Cu-Fe/Al LDO increased with increasing the coating thickness. The effect of the incorporation of Fe/Al LDO nanoparticles on the texture of Cu coatings can also be seen through a comparison of *RTC* coefficients obtained for thicker Cu coatings without and with Fe/Al LDO nanoparticles. Assuming that for 40 μm thick Cu coatings, the eventual effect of substrate on the coating texture was completely avoided, the degree of (220) preferred orientation in the pure Cu coating electrodeposited on Si(111) substrate under the same electrodeposition conditions (*RTC*(220) = 90.7%) [50] was considerably larger than that obtained for Cu-Fe/Al LDO coating (*RTC*(220) = 59.4%). Simultaneously, the *RTC* coefficients for the (111) plane were: for 40 μm thick pure Cu coating – *RTC*(111) = 1.71% [50] and for 50 μm thick Cu-Fe LDO coating – *RTC*(111) = 13.0%. Hence, the addition of Fe/Al

LDO nanoparticles favored an electrodeposition in the "harder" (111) crystal plane with the lowest surface energy for the fcc type of crystal lattice of Cu [42,58].

The addition of Fe/Al LDO nanoparticles led to a transformation of a composite hardness system from a "soft film on hard cathode" to a "hard film on soft cathode" system, signifying a successful incorporation of these particles in the Cu coatings.

The Hall–Petch relationship is usually used to determine the relationship between hardness and crystallite size [59–62]. Regarding crystallite size values, deformation mechanisms in polycrystalline copper can be categorized into three groups: (1) grain shearing and pile-up at grain borders (grain size greater than or equal to 100 nm); (2) shockley (or lattice) partial dislocations (grain sizes between 10 and 100 nm); and (3) grain boundary sliding (grain sizes less than around 10 nm) [59]. Taking into consideration that the average crystallite size (D_{av}) determined by Scherrer's equation [63] was about 30 nm (Figure 11), it is clear that Cu-Fe/Al LDO coatings belong to the second group—Shockley (or lattice) partial dislocations. For this group, the Hall–Petch relationship cannot be applied because the crystallite size was less than 100 nm. Since there is no drastic change in the morphology or crystalline nature of these coatings, the only parameter responsible for the increase in hardness is the incorporation of the nanoparticles in the Cu matrix.

Wenzel's model [56,64] provides an explanation for a variation in the wettability characteristics of Cu coatings. The higher contact angle of Cu-Fe/Al LDO coatings in comparison to the reinforcement-free Cu coating may be due to the existence of bigger grains, microclusters, and protrusions on the top of the coated surface, which can effectively block the attachment of water droplets [65]. The values of contact angle, $\theta_{C,}$ for the Cu-Fe/Al LDO coatings with thicknesses of 20 and 50 μm are very close to each other (99.7–101.7°). The measurement θ_C value for a 10 μm thick Cu-Fe/Al LDO coating was about 30.5% larger than the θ_C obtained for the Cu coating without Fe/Al LDO nanoparticles ($\theta_C = 69.9 \pm 0.54°$). Based on the value of the contact angle, it is clear that the copper coating with the Fe/Al LDO nanoparticles had a hydrophobic character ($\theta_C > 90°$) [12,54], while that obtained without the Fe/Al LDO nanoparticles is of a hydrophilic character ($\theta_C < 90°$).

The surface roughness, the preferred orientation, a distribution of the grain size (height), and the size of crystallites have effects on the hardness values, while only roughness has an impact on the wettability properties of coatings [66,67]. In our case, all listed factors are additionally affected by the change in the coating thickness and by the addition of Fe/Al LDO nanoparticles in the electrolyte. Certainly, it was shown that Fe/Al LDO nanoparticles are successfully incorporated in the Cu coatings, and hence, they can be used as reinforcements for the production of Cu matrix composites.

5. Conclusions

Nanosized particles of Fe/Al LDO were proven to be stable in an acidic sulphate electrolyte. The LDO were obtained from the corresponding LDH particles by calcination.

Cu matrix composites with a thickness of 5, 10, 20, and 50 μm were produced with the incorporation of 0.3 wt.% Fe/Al LDO nanoparticles as reinforcement by the electrodeposition technique and compared with a 10 μm thick pure Cu coating. The effect of Fe/Al LDO nanoparticles on the co-electrodeposition process can be summarized as follows:

- Both Cu and Cu-Fe/Al LDO coatings were fine-grained and microcrystalline, without observable differences in their surface morphology.
- The roughness of Cu-Fe/Al LDO coatings increased with the increase in coating thickness. Comparing a 10 μm thick pure Cu coating with a Cu-Fe/Al LDO coating, an increase in roughness of about 22.0% was observed, which can be attributed to the incorporation of Fe/Al LDO nanoparticles in the Cu coating.
- The use of Fe/Al LDO nanoparticles affected the preferred orientation of the Cu coating: the preferred orientation changed from (111)(220) for the reinforcement-free coatings to (220) for Cu-Fe/Al LDO coatings.

- Hardness analysis of Cu coatings performed by application of the Chicot-Lesage (C-L) composite hardness model showed that the Cu coatings electrodeposited with an addition of Fe/Al LDO nanoparticles showed considerably larger hardness than the coating obtained from the reinforcement-free electrolyte. The addition of Fe/Al LDO nanoparticles in the electrolyte and their incorporation in the Cu matrix during the co-electrodeposition process caused a change in the composite hardness system from "soft film on hard cathode" to "hard film on soft cathode" system.
- The wettability of the Cu coatings changed with the addition of Fe/Al LDO nanoparticles, from hydrophilic (for pure Cu coating) to hydrophobic (for Cu-Fe/Al LDO coatings). The largest effect on this change was the increase in roughness of the coatings caused by the incorporation of nanoparticles.

Based on the performed analyses, it follows that the correlation among the hardness, the wettability, and the surface characteristics of the coatings was successfully established. Hence, Fe/Al LDO nanoparticles can be used as reinforcements in the production of Cu matrix composites by the electrodeposition technique.

Supplementary Materials: The following supporting information can be downloaded at: https://www.mdpi.com/article/10.3390/coatings14060740/s1, Table S1: The values of the composite, H_c and an intrinsic, H_i hardness calculated by application of C–L CHM for pure Cu and Cu-Fe/Al LDO coatings with a concentration of the Fe/Al LDO nanoparticles of 0.3 wt. %. RID-relative indentation depth; *P*-applied load. Reference [68] is cited in the supplementary materials.

Author Contributions: Conceptualization, I.O.M. and N.D.N.; methodology, I.O.M., M.M.V., D.G.V.-R. and R.V.; software, M.M.V. and D.G.V.-R.; validation, R.M.J.H., A.D.M. and N.D.N.; formal analysis, S.S.M.M. and I.O.M.; investigation, S.S.M.M. and I.O.M.; resources, M.M.V.; data curation, M.M.V.; writing—original draft preparation, S.S.M.M., I.O.M. and N.D.N.; writing—review and editing, N.D.N., R.M.J.H., M.M.V., R.V. and A.D.M.; visualization, I.O.M., M.M.V., N.D.N. and D.G.V.-R.; supervision, N.D.N., R.M.J.H., M.M.V. and A.D.M.; funding acquisition, M.M.V. All authors have read and agreed to the published version of the manuscript.

Funding: This research was funded by the Ministry of Science, Technological Development, and Innovation of the Republic of Serbia funded the research (Contracts Nos. 451-03-65/2024-03/200135, 451-03-66/2024-03/200026, 451-03-66/2024-03/200017, and 451-03-66/2024-03/200162).

Institutional Review Board Statement: Not applicable.

Informed Consent Statement: Not applicable.

Data Availability Statement: The data presented in this study are available on request from the corresponding author or co-authors. The data are not publicly available.

Acknowledgments: This research was funded by the Ministry of Science, Technological Development and Innovation of the Republic of Serbia (Contracts Nos. 451-03-65/2024-03/200135, 451-03-66/2024-03/200026, 451-03-66/2024-03/200017, and 451-03-66/2024-03/200162).

Conflicts of Interest: The authors declare no conflicts of interest.

References

1. Alataş, S.; Hiçyılmaz, B.; Karakaya, E. Material demand and material efficiency for sustainable development in the European Union countries: A stochastic frontier analysis. *Sustain. Dev.* **2024**, *32*, 166–183. [CrossRef]
2. Chan, K.-Y.; Tou, T.-Y.; Teo, B.-S. Thickness dependence of the structural and electrical properties of copper films deposited by dc magnetron sputtering technique. *Microelectron. J.* **2006**, *37*, 608–612. [CrossRef]
3. Cho, H.J.; Yan, D.; Tam, J.; Erb, U. Effects of diamond particle size on the formation of copper matrix and the thermal transport properties in electrodeposited copper-diamond composite materials. *J. Alloys Compd.* **2019**, *791*, 1128–1137. [CrossRef]
4. Han, H.; Seo, J.; Kim, Y.; Lee, J.; Park, J.; Yoon, S.; Yoo, B. Electrodeposition of stress-relaxation-induced (111)-oriented nanotwin copper film by direct current in additive-free electrolyte. *Electrochim. Acta* **2024**, *475*, 143694. [CrossRef]
5. Chen, K.-X.; Gao, L.-Y.; Li, Z.; Sun, R.; Liu, Z.-Q. Research Progress of Electroplated Nanotwinned Copper in Microelectronic Packaging. *Materials* **2023**, *16*, 4614. [CrossRef]
6. Han, h.; Lee, C.; Kim, Y.; Lee, J.; Kim, R.; Kim, J.; Yoo, B. Cu to Cu direct bonding at low temperature with high density defect in electrodeposited Cu. *Appl. Surf. Sci. Adv.* **2021**, *550*, 149337. [CrossRef]

7. Zimmerman, A.F.; Palumbo, G.; Aust, K.T.; Erb, U. Mechanical properties of nickel silicon carbide nanocomposites. *Mater. Sci. Eng. A* **2002**, *328*, 137–146. [CrossRef]
8. Li, H.; Xie, Y.; Zhang, L.; Wang, H. Thermal properties of diamond/Cu composites enhanced by TiC plating with molten salts containing fluoride and electroless-plated Cu on diamond particles. *Diamond Relat. Mater.* **2022**, *129*, 109337. [CrossRef]
9. Chang, J.; Zhai, H.; Hu, Z.; Li, J. Ultra-thin metal composites for electromagnetic interference shielding. *Comp. Part B Eng.* **2022**, *246*, 110269. [CrossRef]
10. Meister, T.L.; Fortmann, J.; Breisch, M.; Sengstock, C.; Steinmann, E.; Köller, M.; Pfaender, S.; Ludwig, A. Nanoscale copper and silver thin film systems display differences in antiviral and antibacterial properties. *Sci. Rep.* **2022**, *12*, 7193. [CrossRef]
11. Jiang, F.; Zhu, T.; Kuang, Y.; Wu, H.; Li, S. Superhydrophobic copper coating with ultrahigh corrosion resistance by electrodeposition process in a deep eutectic solvent. *Chem. Phys. Lett.* **2023**, *811*, 140197. [CrossRef]
12. Mladenović, I.O.; Vuksanović, M.M.; Dimitrijević, S.P.; Vasilić, R.; Radojević, V.J.; Vasiljević-Radović, D.G.; Nikolić, N.D. Mechanical Properties of Electrolytically Produced Copper Coatings Reinforced with Pigment Particles. *Metals* **2023**, *13*, 1979. [CrossRef]
13. Chee, C.Y.; Azmi, A. Preparation and characterization of copper/copper coated silicon carbide composites. *Int. J. Precis. Eng. Manuf.* **2014**, *15*, 1215–1221. [CrossRef]
14. Li, Q.; Guo, T.; Liu, L.; Wang, X.; Gao, K.; Pang, X. Orientation controlled microstructure and mechanical properties of TiN-Cu nanocomposite films. *Surf. Coat. Technol.* **2023**, *452*, 129112. [CrossRef]
15. Robin, A.; de Santana, J.C.P.; Sartori, A.F. Co-electrodeposition and characterization of Cu–Si_3N_4 composite coatings. *Surf. Coat. Technol.* **2011**, *205*, 4596–4601. [CrossRef]
16. Yang, G.; Hui, V.; Chen, J.; Li, B.; Chen, J.; Liu, K.; Liang, G.; Deng, D. Effect of discrete Cr nano-nuclei on stripping property and resistivity of ultrathin Cu foil. *Trans. Nonferrous Met. Soc. China* **2023**, *33*, 2698–2711. [CrossRef]
17. Akhtar, K.; Hira, U.; Khalid, H.; Zubair, N. Uniform fine particles of ZrO_2 as reinforcement filler in the electrodeposited Cu-ZrO_2 nanocomposite coating on steel substrate. *J. Alloys Compd.* **2019**, *772*, 15–24. [CrossRef]
18. Pingale, A.D.; Owhal, A.; Katarkar, A.S.; Belgamwar, S.U. Fabrication and tribo-mechanical performance of Cu@Al_2O_3 composite. *Mater. Today Proc.* **2022**, *64*, 1175–1181. [CrossRef]
19. Zhao, J.-C.; Tang, J.-C.; Ye, N.; Zhou, W.-W.; Wei, C.-L.; Liu, D.-J. Influence of additives and concentration of WC nanoparticles on properties of WC−Cu composite prepared by electroplating. *Trans. Nonferrous Met. Soc. China* **2020**, *30*, 1594–1604. [CrossRef]
20. Mo, W.; Yang, Y.; He, C.; Huang, Y.; Feng, J. Excellent adsorption properties of Mg/Al/Fe LDOs for Cr (VI) in water. *J. Environ. Chem. Eng.* **2023**, *11*, 111069. [CrossRef]
21. Bari, G.A.K.M.R.; Kang, H.J.; Lee, T.G.; Hwang, H.J.; An, B.H.; Seo, H.W.; Ko, C.H.; Hong, W.H.; Jun, J.S. Dual-templating-derived porous carbons for low-pressure CO_2 capture. *Carbon Lett.* **2023**, *33*, 811–822. [CrossRef]
22. Kamali, N.; Ghasemi, J.B.; Ziarani, M.M.; Moradian, S.; Badiei, A. Design, synthesis, and nanoengineered modification of spherical graphene surface by layered double hydroxide (LDH) for removal of As(III) from aqueous solutions. *Chin. J. Chem. Eng.* **2023**, *53*, 374–380. [CrossRef]
23. Tian, G.-L.; Zhao, M.-Q.; Zhang, B.; Zhang, Q.; Zhang, W.; Huang, J.-Q.; Chen, T.-C.; Qian, W.-Z.; Su, D.S.; Wei, V. Monodisperse embedded nanoparticles derived from an atomic metal-dispersed precursor of layered double hydroxide for architectured carbon nanotube formation. *J. Mater. Chem. A* **2014**, *2*, 1686–1696. [CrossRef]
24. Liu, Y.; Yang, Z.; Xie, X.; Huang, J.; Wen, X. Layered Double Oxides Nano-flakes Derived from Layered Double Hydroxides: Preparation, Properties and Application in Zinc/Nickel Secondary Batteries. *Electrochim. Acta* **2015**, *185*, 190–197. [CrossRef]
25. Bin, Z.; Wang, Q.; Mo, L.; Jin, F.; Zhu, J.; Tang, M. Synthesis of Mg-Al LDH and its calcined form with natural materials for efficient Cr(VI) removal. *J. Environ. Chem. Eng.* **2022**, *10*, 108605. [CrossRef]
26. Wang, W.; Zhou, J.; Achari, G.; Yu, J.; Cai, W. Cr(VI) removal from aqueous solutions by hydrothermal synthetic layered double hydroxides: Adsorption performance, coexisting anions and regeneration studies. *Colloids Surf. A* **2014**, *457*, 33–40. [CrossRef]
27. Alazreg, A.; Vuksanović, M.M.; Egelja, A.; Mladenović, I.O.; Radovanović, Ž.; Petrović, M.; Marinković, A.; Jančić Heinemann, R. Mechanical properties of acrylate matrix composite reinforced with manganese-aluminum layered double hydroxide. *Polym. Compos.* **2023**, *44*, 6783–6792. [CrossRef]
28. Alazreg, A.; Vuksanović, M.M.; Mladenović, I.O.; Egelja, A.; Janković-Mandić, L.; Marinković, A.; Jančić Heinemann, R. Dental material based on poly(methyl methacrylate) with magnesium-aluminum layered double hydroxide (MgAl-LDH) on bio-silica particles. *Mater. Lett.* **2024**, *354*, 135354. [CrossRef]
29. Mojsilović, K.; Serdechnova, M.; Blawert, C.; Zheludkevich, M.L.; Stojadinović, S.; Vasilić, R. In-situ incorporation of LDH particles during PEO processing of aluminium alloy AA2024. *Appl. Surf. Sci.* **2024**, *654*, 159450. [CrossRef]
30. Li, L. Biomedical Relevant Layered Double Hydroxides as Versatile Drug Carriers and Nanofillers. Ph.D. Thesis, University Medical Center Groningen, University of Groningen, Groningen, The Netherlands, 4 October 2023. [CrossRef]
31. Iankov, R.; Cherneva, S.; Stoychev, D. Investigation of material properties of thin copper films through finite element modelling of microindentation test. *Appl. Surf. Sci.* **2008**, *254*, 5460–5469. [CrossRef]
32. Volinsky, A.A.; Vella, J.; Adhihetty, I.S.; Sarihan, V.; Mercado, L.; Yeung, B.H.; Gerberich, W.W. Microstructure and Mechanical Properties of Electroplated Cu Thin Films. *MRS Online Proc. Lib.* **2000**, *649*, Q5.3.1–Q5.3.6. [CrossRef]
33. Oliver, W.C.; Pharr, G.M. An improved technique for determining hardness and elastic modulus using load and displacement sensing indentation experiments. *J. Mater. Res.* **1992**, *7*, 1564–1583. [CrossRef]

34. Mladenović, I.O.; Nikolić, N.D.; Lamovec, J.S.; Vasiljević-Radović, D.; Radojević, V. Application of the Composite Hardness Models in the Analysis of Mechanical Characteristics of Electrolytically Deposited Copper Coatings: The Effect of the Type of Substrate. *Metals* **2021**, *11*, 111. [CrossRef]
35. Takayama, T. Vickers Hardness Mechanical Models and Thermoplastic Polymer Injection-Molded Products' Static Friction Coefficients. *J. Manuf. Mater. Process.* **2024**, *8*, 11. [CrossRef]
36. Brillon, A.; Heintz, J.-M.; Constantin, L.; Pillier, F.; Lu, Y.; Silvain, J.-F.; Debiemme-Chouvy, C. Anisotropic thermal conductivity and enhanced hardness of copper matrix composite reinforced with carbonized polydopamine. *Compos. Commun.* **2022**, *33*, 101210. [CrossRef]
37. Jin, L.; Zhou, X.; Wang, F.; Ning, X.; Wen, Y.; Song, B.; Yang, C.; Wu, D.; Ke, X.; Peng, L. Insights into memory effect mechanisms of layered double hydroxides with solid-state NMR spectroscopy. *Nat. Commun.* **2022**, *13*, 6093. [CrossRef] [PubMed]
38. Vuksanović, M.M.; Egelja, A.; Barudžija, T.; Tomić, N.; Petrović, M.; Marinković, A.; Radojević, V.; Jančić Heinemann, R. Inorganically modified particles FeAl-LDH@SiO_2 as reinforcement in poly (methyl) methacrylate matrix composite. *R. Soc. Open Sci.* **2021**, *8*, 2108354. [CrossRef]
39. Usoltsev, V.; Tikhov, S.; Salanov, A.; Sadykov, V.; Golubkova, G.; Lomovskii, O. Properties of porous FeAlOy/FeAlx ceramic matrix composite influenced by mechanical activation of FeAl powder. *Bull. Mater. Sci.* **2013**, *36*, 1195–1200. [CrossRef]
40. Robin, M.B.; Day, P. Mixed Valence Chemistry-A Survey and Classification. In *Advances in Inorganic Chemistry and Radiochemistry*, 2nd ed.; Emeléus, H.J., Sharpe, A.G., Eds.; Academic Press: Cambridge, UK, 1968; Volume 10, pp. 247–422. [CrossRef]
41. Zhu, Y.X.; Wang, S.F.; Zhang, Y.S.; Wu, Z.G.; Zhong, B.; Li, D.R.; Wang, F.Y.; Feng, J.J.; Tang, J.; Zhuo, R.F.; et al. Large-scale preparation of Co nanoparticles as an additive in carbon fiber for microwave absorption enhancement in C band. *Sci. Rep.* **2021**, *11*, 2171. [CrossRef]
42. Popov, K.I.; Djokić, S.S.; Nikolić, N.D.; Jović, V.D. *Morphology of Electrochemically and Chemically Deposited Metals*; Springer International Publishing: New York, NY, USA, 2016. [CrossRef]
43. Mladenović, I.O.; Lamovec, J.S.; Vasiljević Radović, D.G.; Vasilić, R.; Radojević, V.J.; Nikolić, N.D. Morphology, Structure and Mechanical Properties of Copper Coatings Electrodeposited by Pulsating Current (PC) Regime on Si(111). *Metals* **2020**, *10*, 488. [CrossRef]
44. Sudha, V.; Murugadoss, G.; Thangamuthu, R. Structural and morphological tuning of Cu-based metal oxide nanoparticles by a facile chemical method and highly electrochemical sensing of sulphite. *Sci. Rep.* **2021**, *11*, 3413. [CrossRef] [PubMed]
45. Mladenović, I.O.; Lamovec, J.S.; Vasiljević-Radović, D.; Radojević, V.; Nikolić, N.D. Determination of the absolute hardness of electrolytically produced copper coatings by application of the Chicot-Lesage composite hardness model. *J. Serb. Chem. Soc.* **2022**, *87*, 899–910. [CrossRef]
46. Chicot, D.; Lesage, J. Absolute Hardness of Films and Coatings. *Thin Solid Film.* **1995**, *254*, 123–130. [CrossRef]
47. Lesage, J.; Chicot, D.; Pertuz, A.; Jouan, P.-Y.; Horny, N.; Soom, A. A Model for Hardness Determination of Thin Coatings from Standard Micro-Indentation Tests. *Surf. Coat. Technol.* **2005**, *200*, 886–889. [CrossRef]
48. Lesage, J.; Pertuz, A.; Puchi-Cabrera, E.S.; Chicot, D. A Model to Determine the Surface Hardness of Thin Films from Standard Micro-Indentation Tests. *Thin Solid Film.* **2006**, *497*, 232–238. [CrossRef]
49. Lamovec, J.; Jović, V.; Randjelović, D.; Aleksić, R.; Radojević, V. Analysis of the Composite and Film Hardness of Electrodeposited Nickel Coatings on Different Substrates. *Thin Solid Film.* **2008**, *516*, 8646–8654. [CrossRef]
50. Mladenović, I.O.; Lamovec, J.S.; Vasiljević-Radović, D.G.; Vasilić, R.; Radojević, V.J.; Nikolić, N.D. Implementation of the Chicot–Lesage Composite Hardness Model in a Determination of Absolute Hardness of Copper Coatings Obtained by the Electrodeposition Processes. *Metals* **2021**, *11*, 1807. [CrossRef]
51. Broitman, E. Indentation Hardness Measurements at Macro-, Micro-, and Nanoscale: A Critical Overview. *Tribol. Lett.* **2017**, *65*, 23. [CrossRef]
52. Sargent, P.M. Indentation size effect and strain-hardening. *J. Mater. Sci. Lett.* **1989**, *8*, 1139–1140. [CrossRef]
53. Chuah, H.G.; Ripin, Z.M. Quantifying the surface roughness effect in microindentation using a proportional specimen resistance model. *J. Mater. Sci.* **2013**, *48*, 6293–6306. [CrossRef]
54. Huhtamäki, T.; Tian, X.; Korhonen, J.T.; Ras, R.H.A. Surface-wetting characterization using contact-angle measurements. *Nat. Protoc.* **2018**, *13*, 1521–1538. [CrossRef]
55. Wang, S.; Feng, L.; Liu, H.; Sun, T.; Zhang, X.; Jiang, L.; Zhu, D. Manipulation of Surface Wettability between Superhydrophobicity and Superhydrophilicity on Copper Films. *Chem. Eur.* **2005**, *6*, 1475–1478. [CrossRef] [PubMed]
56. Marmur, A. Hydro- Hygro- Oleo- Omni-Phobic? Terminology of Wettability Classification. *Soft Matter.* **2012**, *8*, 6867. [CrossRef]
57. Zhang, B.; Xu, W. Superhydrophobic, Superamphiphobic and SLIPS Materials as Anti-Corrosion and Anti-Biofouling Barriers. *New J. Chem.* **2021**, *45*, 15170–15179. [CrossRef]
58. Maharana, H.S.; Panda, S.; Basu, A. Effect of texture and microstructure on properties of electrodeposited Cu-SiO_2 and Cu-Y_2O_3 coatings. *Surf. Coat. Technol.* **2017**, *315*, 558–566. [CrossRef]
59. Hakamada, M.; Nakamoto, Y.; Matsumoto, H.; Iwasaki, H.; Chen, Y.; Kusuda, H.; Mabuchi, M. Relationship between hardness and grain size in electrodeposited copper films. *Mater. Sci. Eng. A* **2007**, *457*, 120–126. [CrossRef]
60. Kao, Y.-J.; Li, Y.-J.; Shen, Y.-A. Significant Hall–Petch effect in micro-nanocrystalline electroplated copper controlled by SPS concentration. *Sci. Rep.* **2023**, *13*, 428. [CrossRef] [PubMed]
61. Hansen, N. Hall–Petch relation and boundary strengthening. *Scr. Mater.* **2004**, *51*, 801–806. [CrossRef]

62. Dao, M.; Lu, L.; Asaro, R.J.; De Hosson, J.T.M.; Ma, E. Toward a quantitative understanding of mechanical behavior of nanocrystalline metals. *Acta Mater.* **2007**, *55*, 4041–4065. [CrossRef]
63. Holzwarth, U.; Gibson, N. The Scherrer equation versus the 'Debye-Scherrer equation'. *Nat. Nanotechnol.* **2011**, *6*, 534. [CrossRef]
64. Wenzel, R.N. Resistance of Solid Surfaces to Wetting by Water. *Ind. Eng. Chem.* **1936**, *28*, 988–994. [CrossRef]
65. Feng, L.; Li, S.; Li, Y.; Li, H.; Zhang, L.; Zhai, J.; Song, Y.; Liu, B.; Jiang, L.; Zhu, D. Super-Hydrophobic Surfaces: From Natural to Artificial. *Adv. Mater.* **2002**, *14*, 1857–1860. [CrossRef]
66. Dong, J.; Liu, Y.; Pacella, M. Surface Texturing and Wettability Modification by Nanosecond Pulse Laser Ablation of Stainless Steels. *Coatings* **2024**, *14*, 467. [CrossRef]
67. Wu, P.; Xue, Z.; Yu, T.; Penkov, O.V. Transparent Self-Cleaning Coatings: A Review. *Coatings* **2023**, *13*, 1270. [CrossRef]
68. Nikolić, N.D.; Maksimović, V.M.; Avramović, L. Correlation of Morphology and Crystal Structure of Metal Powders Produced by Electrolysis Processes. *Metals* **2021**, *11*, 859. [CrossRef]